Preparation and characterization of strontium-doped bismuth borate glasses

Yu. S. Hordieiev*, A. V. Zaichuk
Ukrainian State University of Chemical Technology, 8 Gagarin Avenue, Dnipro, 49005, Ukraine

Employing the melt quenching method, new bismuth borate glass compositions denoted as $(40+x)Bi_2O_3$–$(60-x-y)B_2O_3$–ySrO, with x and y ranging between 0 to 20 mol%, were synthesized. The X-ray Diffraction analyses confirmed the amorphous nature of all glass samples, indicating the absence of long-range order typically seen in crystalline materials. Concurrently, the Fourier-transform Infrared Spectroscopy examinations unveiled the existence of fundamental structural units within the glasses, including BO_3 and BO_4 trigonal and tetrahedral units, as well as BiO_3 and BiO_6 polyhedra, suggesting a complex network structure. Differential Thermal Analysis (DTA) and dilatometry assessed the glasses' thermal properties. DTA demonstrated the glasses' high thermal stability, with a stability value of up to 106°C, noting that stability improves with more SrO. Dilatometry analyses revealed these glasses exhibit a high thermal expansion coefficient, ranging from 8.69 to 10.7 ppm/°C, alongside relatively low glass transition temperatures between 362 and 432°C and dilatometric softening temperatures spanning from 380 to 447°C. Density measurements were conducted, followed by molar volume and oxygen packing density calculations, to glean further insights into the samples. Compared to other heavy-metal oxide glasses, the glasses examined in this study exhibited notably high-density values, ranging between 6.279 and 7.476 g/cm^3.

(Received March 18, 2024; Accepted May 27, 2024)

Keywords: Glass, Glass transition, Thermal stability, Thermal expansion, Density

1. Introduction

Heavy metal oxide glasses are a notable subject of interest within the field of materials science, primarily because of their exceptional versatility and extensive applicability across various domains. They possess exceptional optical properties, such as the ability to transmit infrared light while maintaining high transparency in the visible spectrum, making them ideal for use in various optical components, including lenses, windows and fibers used in telecommunications and laser technologies [1, 2]. Furthermore, their high density and capacity for absorbing ionizing radiation position them as optimal materials for protective barriers against gamma and X-ray radiation, making them invaluable in medical imaging, radiation biology, nuclear facilities, and aerospace applications [3, 4]. The low melting point of heavy metal oxide glasses [5], relative to traditional glass, facilitates easier manufacturing processes, enabling the creation of complex shapes and sizes without compromising material integrity [6]. This characteristic, along with their chemical stability and durability, also makes them suitable for encapsulating high-level nuclear waste, providing a safe and long-term solution for radioactive material storage [7]. The non-linear optical properties of these glasses open the door to cutting-edge applications in all-optical switching and modulation devices, which are crucial for next-generation optical computing and information processing technologies [8].

Bismuth borate glasses are notable among heavy metal oxide glasses for their high transparency in the visible and near-infrared regions, broad range of glass formation, and excellent solubility for rare-earth ions [9]. Combining bismuth oxide with boron oxide yields glasses with high refractive indices and densities, making them promising candidates for advanced optical applications and radiation shielding materials [10]. Bismuth borate glasses are also appreciated for

* Corresponding author: yuriihordieiev@gmail.com
https://doi.org/10.15251/DJNB.2024.192.773

their non-toxic nature, positioning them as potential alternatives to lead-based glasses in various applications.

Doping bismuth borate glasses with strontium (SrO) introduce a series of enhancements to their already impressive characteristics. Strontium doping has been shown to improve the thermal stability, chemical durability, and optical performance of heavy metal oxide glasses, making them even more versatile [11–13]. The addition of SrO modifies the glass network, enhancing the glass-forming ability and preventing devitrification [14]. As a result, glasses doped with SrO exhibit higher glass transition and crystallization temperatures, along with elevated refractive indices and thermal expansion coefficients [12, 15]. Incorporating SrO in bismuth borate glasses thus opens up new avenues for developing advanced optical components and protective materials against radiation, highlighting the continuous innovation and exploration within the field of heavy metal oxide glasses.

Overall, heavy metal oxide glasses, with a focus on bismuth borate glasses and the impact of strontium doping, represent a vital area of research and development. Their broad spectrum of applications, from optical and electronic devices to medical and biological uses, underscores the importance of understanding and improving their properties for future technological advancements.

This study's primary goal is to comprehensively analyze how varying the SrO content affects the structural characteristics, crystallization behaviors, thermal stability, and several pivotal physical properties of bismuth borate glasses. This research has synthesized and characterized a glass system with compositions of $(40+x)Bi_2O_3–(60-x-y)B_2O_3–ySrO$ (where $0 \leq x, y \leq 20$ mol%) using techniques such as XRD, FTIR, SEM, DTA, and dilatometry.

2. Materials and methods

Table 1 outlines the glass compositions and designations being examined. Throughout this research, the traditional melt quench technique was applied to create glasses with the formula $(40+x)Bi_2O_3–(60-x-y)B_2O_3–ySrO$, adjusting the x and y values between 0 and 20 mol% to explore different compositions. The glass synthesis involved the use of high-grade raw materials, specifically bismuth oxide (99.9% purity, sourced from Sigma–Aldrich), boric acid (99.9% purity, obtained from Eti Mine Works), and strontium carbonate (99.96% purity, provided by Reachim). These were precisely measured, mixed to ensure even distribution, and melted in a platinum (Pt) crucible within an electric furnace at 1000°C for 45 minutes, providing uniform heat and ensuring thorough melting and homogenization. Afterward, the molten glass was carefully poured into a preheated stainless steel mold [16, 17]. The newly formed glass samples underwent annealing in a muffle furnace at 360°C for five hours to relieve internal stresses. The annealing was followed by a controlled cooling phase, decreasing the temperature at a rate of 30°C per hour to room temperature, which is crucial for enhancing the structural integrity of the glass samples [16].

Table 1. Detailed chemical composition and assigned sample codes of investigated glasses (expressed in Mole Percent).

Sample code	Bi_2O_3	B_2O_3	SrO
60Bi40B	60	40	0
50Bi50B	50	50	0
40Bi60B	40	60	0
40Bi50B10Sr	40	50	10
40Bi45B15Sr	40	45	15
40Bi40B20Sr	40	40	20
50Bi40B10Sr	50	40	10
46Bi46B7Sr	46.5	46.5	7
44Bi44B12Sr	44	44	12
44Bi52B4Sr	44	52	4
52Bi44B4Sr	52	44	4

For differential thermal analysis (DTA), glass samples were finely ground using an agate mortar and pestle [17]. Particles passing through a 270-mesh sieve were used for DTA, conducted in a Derivatograf Q-1500D with Pt crucibles [16]. The samples, alongside a high-purity Al_2O_3 reference, were heated at 5°C per minute from room temperature to 1000°C in air. Key temperatures indicating thermal behavior – glass transition (T_g), crystallization onset (T_x), and crystallization peak (T_c) – were determined from the DTA curve; T_g corresponded to the first endothermic shift, T_x to the initial exothermic change, and T_c to the exothermic peak's maximum [16]. Further, to identify any crystalline phases formed, the powder was heated at T_c for 5 hours and analyzed using X-ray diffraction with a DRON-3M (Co-Kα radiation, λ = 1.79026 Å), and a MIRA3 TESCAN FESEM to examine the phases' morphology [16–18].

In addition to thermal analysis, the study encompassed the acquisition of infrared spectra using a Thermo-Nicolet Avatar 370 FT-IR Spectrometer [16, 17]. Spectra covered 1500 to 400 cm^{-1} with 2 cm^{-1} resolution. Samples were prepared by blending glass powder with potassium bromide (KBr) and pressing into 13 mm pellets [17].

Thermal properties, including softening point (T_d), T_g, and thermal expansion coefficient (CTE), were measured with a DILA GT-1300 dilatometer at a 3°C per minute heating rate [16–18]. Moreover, the density of the glass was accurately measured at room temperature using distilled water [17], employing the Archimedes principle. This procedure was repeated multiple times to ensure accuracy, resulting in a maximum uncertainty range between 0.008 and 0.015 g/cm^3.

3. Results and discussion

In the present study, XRD analysis was employed to examine the structural characteristics of glass samples, with the results depicted in Figure 1. The XRD patterns were meticulously recorded over a 2θ range extending from 10° to 90°. A critical observation from these patterns is the notable absence of sharp, distinct peaks, which are typically indicative of crystalline structures. Instead, the patterns are characterized by a significant broad hump centered at 33°. This feature strongly suggests the amorphous nature of the glass samples being examined. The presence of such a broad hump is indicative of short-range atomic order within an otherwise disordered structure, which is a distinguishing characteristic of amorphous materials [16, 17]. This contrasts significantly with the well-defined, sharp diffraction peaks that are the hallmark of crystalline materials, highlighting the fundamental structural differences between amorphous and crystalline states.

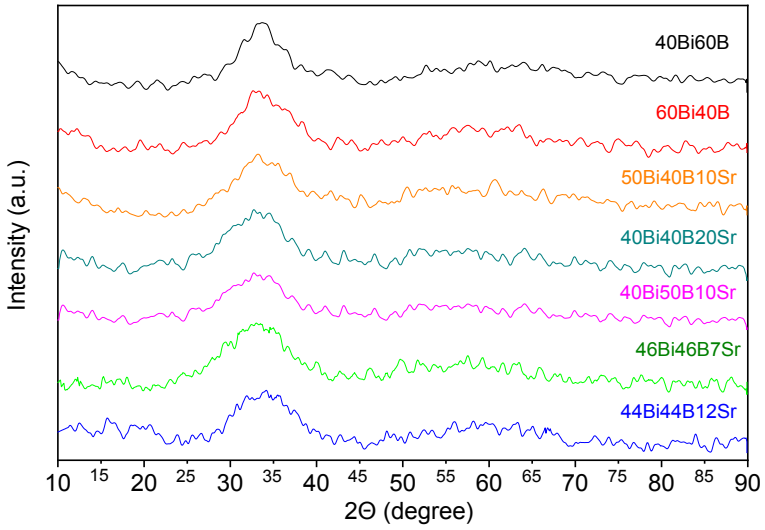

Fig. 1. XRD results of the prepared (40+x)Bi_2O_3–(60-x-y)B_2O_3–ySrO glass samples.

In the investigation of the local structural characteristics of the glasses under study, Fourier Transform Infrared (FT-IR) absorption spectroscopy was employed. The FT-IR spectral analysis shown in Figure 2a confirms that the addition of strontium oxide significantly alters the local structure of bismuth borate glass. Analysis of the FT-IR spectra identified four principal absorption bands (400–600, 700, 800–1100, and 1150–1450 cm^{-1}), with their intensities varying according to the composition of the glass. The broad bands observed in Figure 2a are attributed to the superposition of multiple overlapping bands. To accurately pinpoint the peak positions within the FTIR spectra of the 40Bi60B, 60Bi40B and 40Bi40B20Sr glass samples, a deconvolution process was applied using the Peak Deconvolution module in OriginPro software, employing a Gaussian distribution function for the analysis. The deconvoluted peaks, representing the refined spectral data for these samples, are showcased in Figure 2b, providing a clearer insight into the structural implications of SrO addition to the bismuth borate glass matrix.

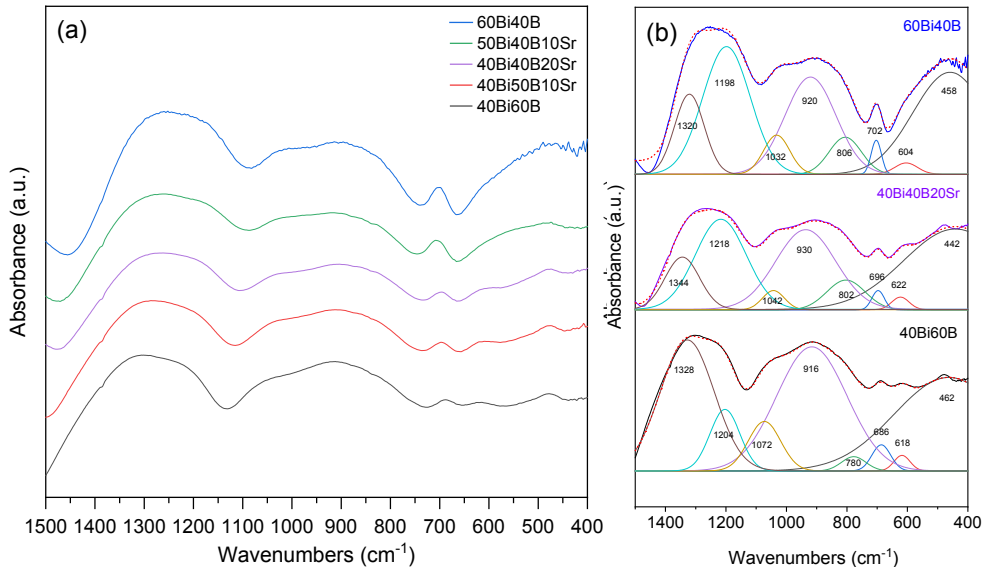

Fig. 2. FT-IR results and deconvolution analysis of the bismuth borate glasses modified by SrO.

The process of analyzing FT-IR spectra and identifying specific absorption bands necessitated a comprehensive review of the existing scholarly work on bismuth borate and strontium borate glasses [19–23]. Borate-based glasses are known for their complex structure, mainly comprising various boron-oxygen (B_xO_y) structural groups. The distinctive properties of these glasses are largely shaped by the addition of various modifiers, which alter the type and distribution of the B_xO_y structural units within the glass matrix [24]. Particularly noteworthy is the role of bismuth oxide in these compositions. Serving as a conditional glass former, bismuth oxide (Bi_2O_3) is instrumental in the development of unique structural formations, such as the pyramidal network former BiO_3 units and the octahedral network modifier BiO_6 units [19]. Figure 2b showcases the results of deconvoluting the FT-IR spectra of the 40Bi60B glass, revealing eight distinct peaks located at 1328, 1204, 1072, 916, 780, 686, 618, and 462 cm^{-1}. It's important to highlight that many of these identified peaks align with findings from earlier research by Varsamis et al. [19], who extensively explored the structural intricacies of bismuth-containing borate glasses. The absorption peak within the 1344–1320 cm^{-1} range is predominantly associated with the asymmetric stretching vibrations of the B–O and B–Ø bonds found within the BO_3 and $BO_2Ø$ units [16, 22], respectively. Here, Ø signifies a non-bridging oxygen atom. This peak's intensity tends to decrease with the equimolar substitution of B_2O_3 for SrO. Adjacent to this, a significant band near 1204 cm^{-1} emerges more prominently as B_2O_3 is substituted by SrO and Bi_2O_3. This enhancement is attributed to the stretching vibrations of B–O bonds within BO_3 units [22] across various borate configurations (meta-, pyro-, and orthoborate) [16]. This indicates a reorganization

of the borate network, influenced by the incorporation of SrO and Bi_2O_3. The third distinct band, observed around 1072–1032 cm^{-1}, is related to B–O stretching vibrations in BO_4 tetrahedral units from tri-, tetra-, and penta-borate groups [25]. The pronounced absorption near 920 cm^{-1} is attributed to both Bi–O symmetric stretching vibrations within BiO_3 pyramidal units and B–O bond stretching in BO_4 tetrahedra present in diborate groups [26, 27]. The marked absorption at 806-780 cm^{-1} suggests that boroxol rings exist in the glass network [28]. The absorption at 686 cm^{-1}, shifting to 702 cm^{-1} with an increase in Bi_2O_3 content, corresponds to B–O–B bending vibrations in BO_3 triangles [29], possibly affected by the electrostatic field from Bi^{2+} ions, as observed by Cheng et al. [30]. The band near 618 cm^{-1} is linked to Bi–Ø stretching vibrations in BiO_6 octahedral units [29], while the final absorption band around 460 cm^{-1} points to the stretching vibrations of Bi–O bonds in highly distorted BiO_6 octahedral configurations [21].

Table 2. Density (ρ), molar volume (V_m), oxygen packing density (OPD) and thermal characteristics of (40+x)Bi_2O_3–(60-x-y)B_2O_3–ySrO glasses.

Sample code	ρ, (g/cm^3)	V_m, (cm^3/mol)	OPD (mol/L)	DTA				Stability parameters			
				T_g, °C	T_x, °C	T_c, °C	T_m, °C	ΔT, °C	K_{SP}	K_H	T_{gr}
60Bi40B	7.476	41.1	73.0	362	420	429	680	58	1.44	0.27	0.53
50Bi50B	6.862	39.0	76.9	395	436	448	670	41	1.25	0.24	0.59
40Bi60B	6.279	36.3	82.6	428	520	555	760	92	7.52	0.62	0.56
40Bi50B10Sr	6.435	36.0	77.9	409	505	538	765	96	7.75	0.53	0.53
40Bi45B15Sr	6.521	35.8	75.5	395	488	522	795	93	8.01	0.47	0.50
40Bi40B20Sr	6.607	35.6	73.1	388	476	493	772	88	3.86	0.38	0.50
50Bi40B10Sr	7.026	38.6	72.6	375	443	467	753	68	4.35	0.32	0.50
46Bi46B7Sr	6.849	37.4	76.4	390	496	506	720	106	2.72	0.54	0.54
44Bi44B12Sr	6.840	36.3	76.1	388	495	507	780	105	3.79	0.44	0.50
44Bi52B4Sr	6.564	37.4	78.1	405	488	513	676	83	5.12	0.66	0.60
52Bi44B4Sr	7.075	39.2	74.5	375	447	469	658	72	4.22	0.50	0.57

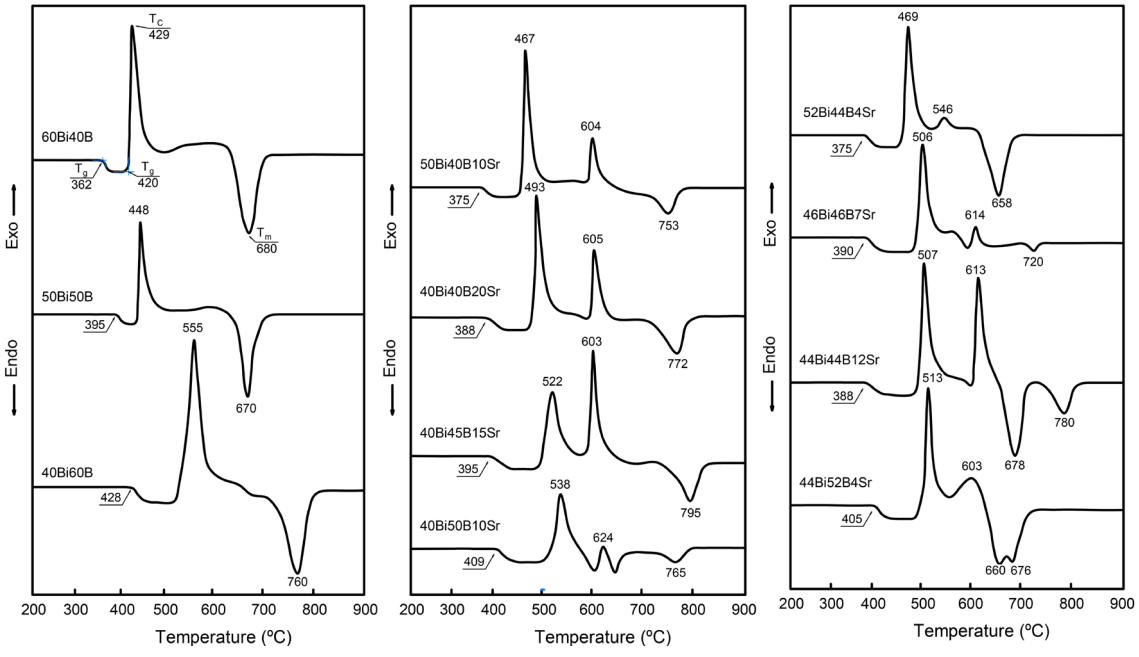

Fig. 3. DTA thermograms for (40+x)Bi_2O_3–(60-x-y)B_2O_3–ySrO glass system.

The investigation into the thermal and crystallization features of oxide glasses is paramount for both grasping their inherent characteristics and unlocking their vast potential for various applications. Among the array of analytical methods, Differential Thermal Analysis (DTA) stands out for its significant contribution to studying the thermal behavior of various substances, with glasses being a notable focus. This method is instrumental in revealing how these materials react to variations in temperature, a knowledge that is crucial for scientific understanding and practical applications alike. The DTA curves depicted in Figure 3 provide a comprehensive overview of key temperatures that define the glass's thermal and crystallization behavior. Table 2 compiles these characteristic temperatures (T_g, T_x, T_c, and T_m (melting point)), as determined from the DTA findings.

DTA curves of the glasses under investigation show consistent thermal patterns, starting with a pronounced endothermic transition followed by a significant exothermic peak. The research findings highlight the impact of compositional adjustments on the thermal properties of glasses. Specifically, replacing B_2O_3 with SrO in the 40Bi60B composition lowers the glass transition and crystallization temperatures (T_x, T_c), while increasing the melting point (T_c). Conversely, substituting Bi_2O_3 for SrO in the 60Bi40B composition raises T_g, T_x, and T_c temperatures but lowers T_m. The addition of SrO to the glass introduces a more intricate crystallization behavior, evidenced by two exothermic peaks on the DTA curves, suggesting the emergence of two distinct crystalline phases. Detailed temperature analysis shows varied peak crystallization temperatures across the compositions: 555°C for 40Bi60B, 429°C for 60Bi40B, and two intense peaks at 493°C and 605°C for 40Bi40B20Sr. Subsequent to this analysis, the glass powders underwent a five-hour heat treatment at their peak crystallization temperatures, followed by phase characterization through powder diffraction file analysis. The XRD results, illustrated in Figure 4, provide insight into the crystalline structures formed post-heat treatment. For the base glass composition 40Bi60B, the XRD analysis post-treatment at 555°C shows the formation of a singular crystalline phase, specifically $Bi_6B_{10}O_{24}$ (PDF 01-070-0154). In the case of the 60Bi40B sample, heating led to the emergence of the $Bi_4B_2O_9$ crystalline phase (PDF 01-070-1458). For the 40Bi40B20Sr composition, the XRD analysis detected the presence of both $Bi_4B_2O_9$ and $Bi_6B_{10}O_{24}$ crystalline phases, consistent with the dual peak temperatures observed at 493°C and 605°C.

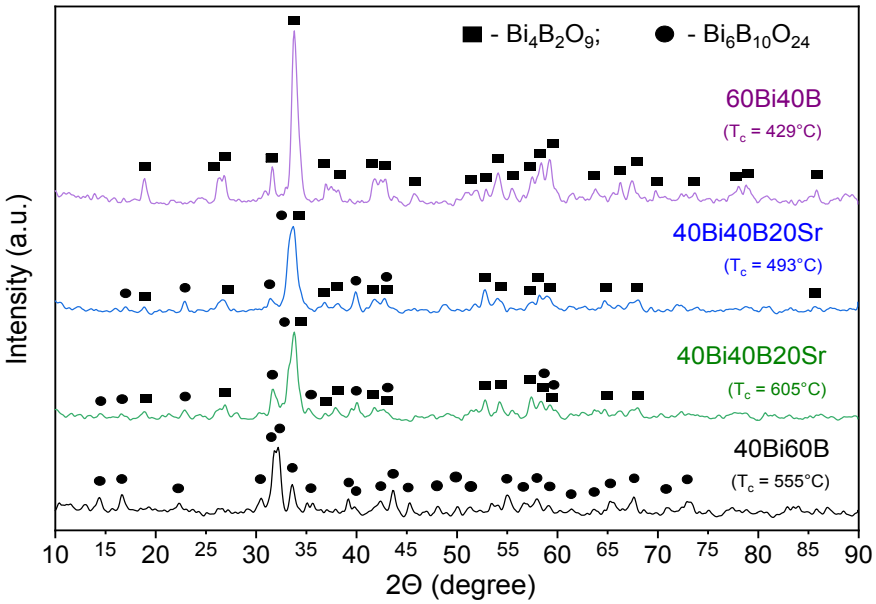

Fig. 4. XRD results of glass powders after undergoing a 5-hour heat treatment process at the temperature corresponding to the peak of crystallization (T_c).

SEM imaging (Fig. 5) of the 60Bi40B glass-ceramic sample highlights the fibrous, needle-like structure of $Bi_4B_2O_9$ crystals, which collectively resemble woven fibers, varying in density across different areas. The morphology of the crystals within this 40Bi40B20Sr sample, which contains 20 mol% SrO, displays a variety of shapes and sizes of crystals embedded in an amorphous matrix. There are needle-like crystals, which are long and thin, alongside some rounded formations. These diverse morphologies suggest a complex crystallization process influenced by the presence of SrO, leading to the heterogeneous nucleation and growth of different crystal phases. The 40Bi60B sample features elongated, rod-like crystals and smaller, more equiaxed forms with rounded or polyhedral shapes, possibly indicating different crystallization stages.

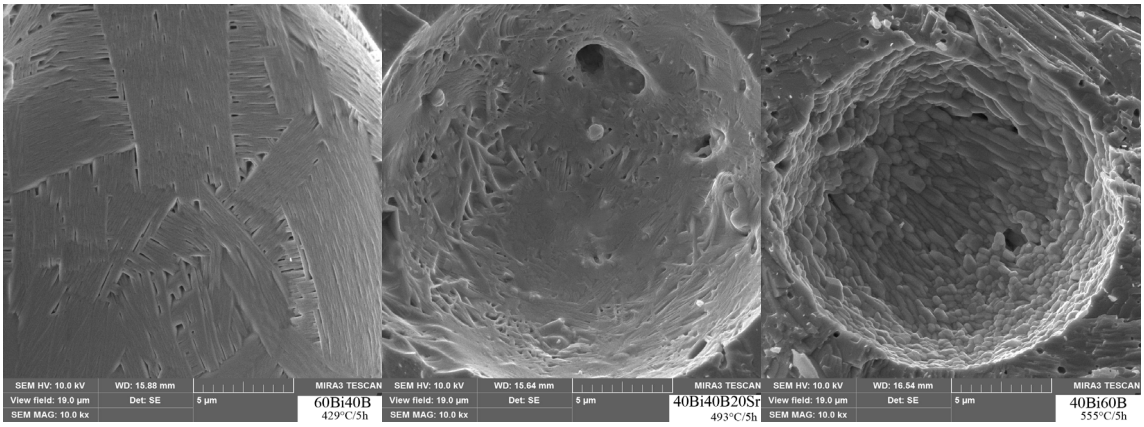

Fig. 5. SEM micrographs depicting the fracture surfaces of samples designated 60Bi40B, 40Bi40B20Sr, and 40Bi60B after heat treatment for five hours.

Glass stability (GS) and glass forming ability (GFA) are crucial characteristics for understanding and predicting the behavior of glass materials during cooling and heating. GFA refers to a material's resistance to crystallization upon cooling from a melt, determining its ability to form a glass without crystallizing. GS, on the other hand, measures a glass's resistance to devitrification upon heating [16], which is crucial for processes like annealing or tempering [31]. Parameters like ΔT (T_x - T_g), K_H ((T_c - T_g)/(T_m - T_c)), K_{SP} ((T_c - T_x)$\Delta T/T_g$), and T_{rg} (T_g/T_m) are commonly used to quantify glass stability, providing insights into the material's ability to retain its amorphous structure under different conditions. The Dietzel criterion [32], ΔT, offers a straightforward measure of glass stability by quantifying the temperature difference between the T_x and T_g temperatures. A larger ΔT value indicates greater thermal stability, suggesting that the glass can withstand higher temperatures without undergoing crystallization. This parameter is valuable for determining the sintering window, which denotes the temperature range [17] within which the glass can be processed without crystallization occurring.

Incorporating SrO into the bismuth borate glass composition significantly improves thermal stability, as evidenced by a significant increase in ΔT from 41 to 107°C. Additionally, the Saad and Poulain criterion [33], represented by K_{SP}, further enriches our understanding by offering insights into the glass's resistance to devitrification and its ability to maintain amorphous structure under thermal stress. This criterion complements the Dietzel criterion by offering a more comprehensive understanding of the glass's behavior during heating, thus aiding in the optimization of processing conditions for glass manufacturing and applications. The introduction of SrO in place of Bi_2O_3 and B_2O_3 significantly increases K_{SP} values, indicating improved thermal stability and more robust resistance to crystallization during thermal treatment. Hruby's parameter (K_H), another crucial metric, evaluates both the GFA and thermal stability of glass. Essentially, Hruby's theory suggests that a higher K_H value signifies a greater resistance to crystallization when the glass is heated and, consequently, a better ability to maintain its amorphous state during cooling. Creating glasses with a K_H value of 0.1 or lower is difficult, necessitating swift cooling

techniques, while those with a K_H value of 0.5 or higher can be more readily produced using moderate cooling rates [34]. The investigated glasses have K_H values ranging from 0.24 to 0.66, indicating moderate to high ease of formation and stability against crystallization. Lastly, the reduced glass transition temperature (T_{rg}), used to predict GFA, shows values between 0.5 and 0.6 in this research, aligning with the Kauzmann criteria ($0.5 \leq T_{rg} \leq 0.66$) [35]. This compliance indicates that the glass compositions examined possess commendable glass-forming capabilities, underscoring the potential for high-quality glass development.

Dilatometry remains an indispensable technique for exploring the thermal performance of glass. It provides essential data (Fig. 6a) on the thermal expansion (coefficient of linear thermal expansion, CTE), T_g, and T_d. These properties are vital for determining a glass's suitability for diverse applications, especially as the oxide composition of glass significantly influences its thermal behavior. Understanding these interactions allows for tailoring glass formulations to meet specific industrial or technological requirements.

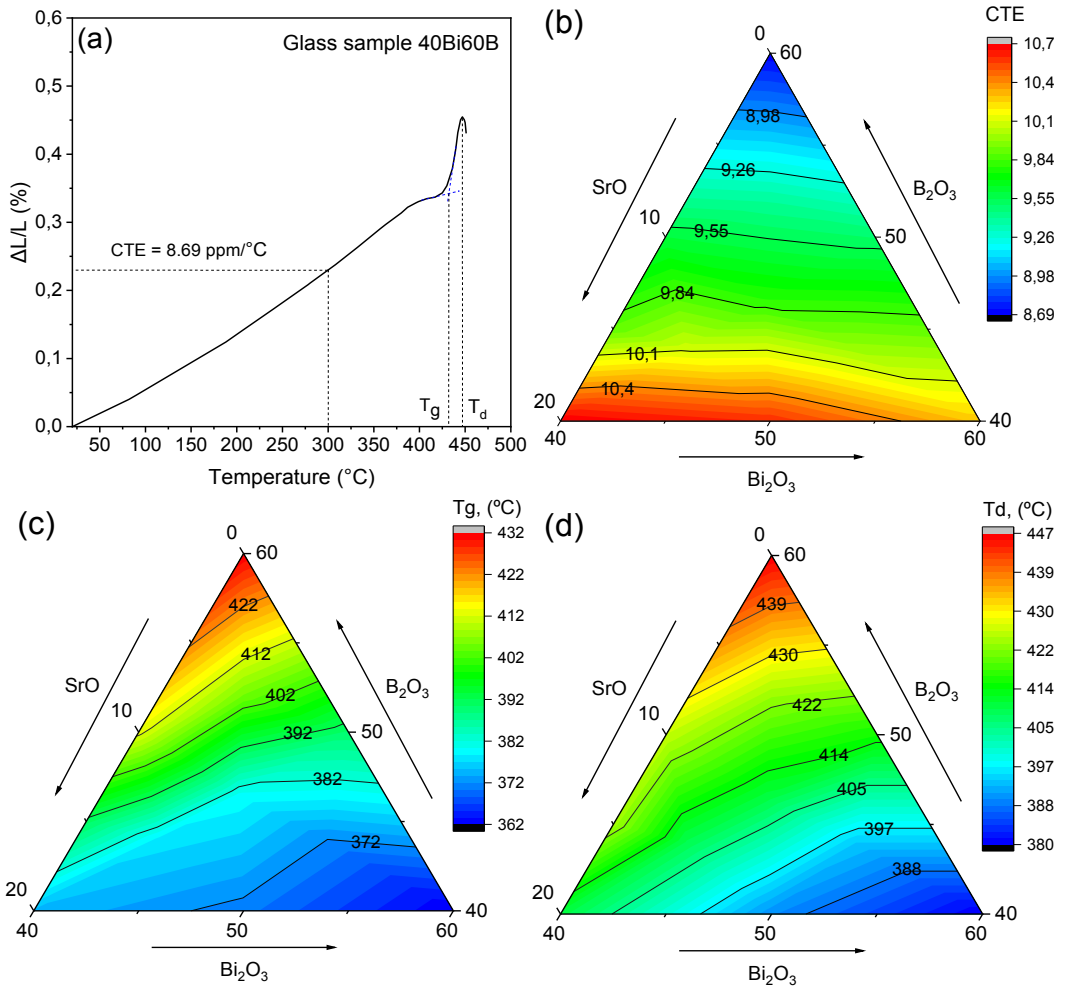

Fig. 6. Dilatometry results for 40Bi60B sample (a), alongside ternary diagrams that illustrate the variations in the CTE (b), T_g (c), and T_d (d) across different compositions within the (40+x)Bi_2O_3–(60-x-y)B_2O_3–ySrO system.

The data presented in Figure 6b-d offers an extensive evaluation of the impact of compositional changes in the (40+x)Bi_2O_3–(60-x-y)B_2O_3–ySrO system on key thermal properties of the glass. Specifically, the analysis demonstrates how altering the ratios of B_2O_3, SrO, and Bi_2O_3 in the 40Bi60B glass matrix significantly modifies the glass's thermal characteristics. The introduction of equimolar amounts of SrO and Bi_2O_3 in place of B_2O_3 leads to notable shifts in

temperature T_g, which decreases markedly from 432°C to 362°C, and T_d, which falls from 447°C to 380°C, as observed in Figures 6c and 6d respectively. Concurrently, the CTE increases from 8.69 ppm/°C to 10.7 ppm/°C (Fig. 6b). This behavior is attributed to the chemical nature of the bonds formed by the substituting oxides: the original B−O bonds in the glass matrix, known for their high strength and rigidity (with a bond energy of 372 kJ/mol) [36], are replaced by the significantly less strong Sr−O (138 kJ/mol) and Bi–O (102 kJ/mol) bonds [5]. This substitution results in a diminished overall network strength, leading to the observed changes in thermal properties. The study underscores the importance of understanding these changes, especially considering the typical CTE values (ranging from 7–12 ppm/ºC) required for glasses used as sealants in optoelectronic packaging and Low-Temperature Co-fired Ceramics applications [9]. The fact that all the glasses analyzed in this study exhibit CTE values within this desirable range is a critical finding, underscoring their potential suitability for such applications.

Investigating changes in the structural configuration of glass through the estimation of critical parameters such as density, oxygen packing density, and molar volume provides a comprehensive insight into the fundamental properties of glass. These metrics indicate changes in the glass network, revealing shifts in compactness, cross-link density, coordination number, and the configuration and size of interstitial spaces within the structure [37]. To comprehensively investigate these variations in strontium-doped bismuth borate glasses, the following calculations of the main parameters were performed: density is calculated by $\rho = W_{air}/(W_{air} - W_{liq})$, molar volume by $V_m = (\Sigma x_i M_i)/\rho$, and oxygen packing density by $OPD = 1000C/V_m$. Here, W_{air} and W_{liq} are the glass's weights in air and distilled water, respectively [38], M_i and x_i represent the molecular weights and molar fractions of components [39], and C is the number of oxygen atoms at each glass composition [39]. The substitution of B_2O_3 with SrO raises the glass density from 6.279 to 6.607 g/ cm^3, and its replacement with Bi_2O_3 increases it further to 7.476 g/cm^3. This variation underscores the additive effect of the oxides' densities: B_2O_3 (ρ = 2.46 g/cm^3) < SrO (ρ = 4.70 g/cm^3) < Bi_2O_3 (ρ = 8.90 g/cm^3). As illustrated in Table 2, substituting B_2O_3 with SrO leads to a decrease in V_m from 36.3 to 35.6 cm^3/mol (contrary to the density trend), while replacing it with Bi_2O_3 mirrors the density's direct trend, indicating an increase from 36.3 to 41.1 cm^3/mol. Substituting B_2O_3 with SrO reduces molar volume due to bridging oxygen formation, resulting in a denser glass structure with minimized vacant spaces. Conversely, increasing Bi_2O_3 content introduces more non-bridging oxygen, increasing V_m by reducing structural compactness and increasing the count of voids. The observed reduction in OPD supports this phenomenon.

4. Conclusions

Low-temperature bismuth borate glasses, doped with varying concentrations of strontium, were synthesized with precision and thoroughly characterized. The glasses were prepared with the compositions $(40+x)Bi_2O_3–(60-x-y)B_2O_3–ySrO$, where x and y values were set at 0, 4, 7, 10, 12, 15, and 20 mol%. A variety of sophisticated analytical techniques including DTA, XRD, SEM, FT-IR and Dilatometry were employed to characterize these materials comprehensively.

The evaluations via XRD and DTA corroborated the glasses' amorphous nature. FT-IR analysis revealed that SrO addition leads to the conversion of BO_3 to BO_4 units, signifying a reduction in non-bridged oxygen atoms and suggesting enhanced structural compactness. Such a structural rearrangement was substantiated by the observed increase in glass density, which rose from 6.279 to 6.607 g/cm^3. Concurrently, there was a slight reduction in molar volume from 36.3 to 35.6 cm^3/mol, attributing these changes to the equimolar substitution of B_2O_3 with SrO that fostered a denser glass structure through an increased presence of bridging oxygen atoms.

Moreover, these compositional modifications not only enhanced the density of the glass structure through a greater number of bridging oxygen atoms but also improved the thermal properties. DTA and dilatometry revealed that substituting B_2O_3 with SrO and increasing the Bi_2O_3 content enhanced the thermal stability of the glasses. The most thermally stable composition was found to be $46.5Bi_2O_3–46.5B_2O_3–7SrO$, with a peak thermal stability ΔT of 106°C. This adjustment also led to a significant alteration in the T_g, which decreased from 432°C to 362°C, and a reduction in the T_d from 447°C to 380°C.

In conclusion, incorporating SrO into bismuth borate glasses significantly enhances their structural, physical, and thermal properties. This leads to potential advancements in glass materials, offering promising characteristics for specialized applications such as optical and electronic devices.

References

[1] D. Lezal, J. Pedlikova, P. Kostka, J. Bludska, M. Poulain, J. Zavadil, J. Non Cryst. Solids. **284**, 288 (2001); https://doi.org/10.1016/S0022-3093(01)00425-2
[2] B. V. Padlyak, I. I. Kindrat, Y. O. Kulyk, S. I. Mudry, A. Drzewiecki, Y. S. Hordieiev, V. I. Goleus, R. Lisiecki, Mater. Sci. Eng. B Solid State Mater. Adv. Technol. **278**, 115655 (2022); https://doi.org/10.1016/j.mseb.2022.115655
[3] P. Kaur, D. Singh, T. Singh, Nucl. Eng. Des. **307**, 364 (2016); https://doi.org/10.1016/j.nucengdes.2016.07.029
[4] A. N. D'Souza, N. S. Prabhu, K. Sharmila, M. I. Sayyed, H. M. Somshekarappa, G. Lakshminarayana, S. Mandal, S. D. Kamath, J. Non Cryst. Solids. **542**, 120136 (2020); https://doi.org/10.1016/j.jnoncrysol.2020.120136
[5] Y. S. Hordieiev, A. V. Zaichuk, Results in Materials **19**, 100442 (2023); https://doi.org/10.1016/j.rinma.2023.100442
[6] A. V. Nosenko, Y. S. Hordieiev, V. I. Goleus, Voprosy Khimii i Khimicheskoi Tekhnologii **1**, 87 (2018).
[7] N. A. Elalaily, E. M. Abou-Hussien, E. A. Saad, Radiat. Eff. Defects Solids. **171**, 840 (2016); https://doi.org/10.1080/10420150.2016.1250093
[8] B. V. Padlyak, I. I. Kindrat, Y. O. Kulyk, Y. S. Hordieiev, V. I. Goleus, R. Lisiecki, Mater. Res. Bull. **158**, 112071 (2023); https://doi.org/10.1016/j.materresbull.2022.112071
[9] T. Maeder, Int. Mater. Rev. **58**, 3 (2013); https://doi.org/10.1179/1743280412Y.0000000010
[10] Y. S. Rammah, M. I. Sayyed, A. A. Ali, H. O. Tekin, R. El-Mallawany, Appl. Phys. A **124**, 832 (2018); https://doi.org/10.1007/s00339-018-2252-7
[11] E. M. A. Hussein, A. M. Madbouly, N. A. E. Alaily, J. Non Cryst. Solids. **570**, 121021 (2021); https://doi.org/10.1016/j.jnoncrysol.2021.121021
[12] Z. Wu, M. Zhang, C. Zhang, F. Meng, H. Lin, J. Wuhan Univ. Technol.-Mat. Sci. Edit. **35**, 368 (2020); https://doi.org/10.1007/s11595-020-2266-9
[13] L. Zhang, Q. Sun, J. Wang, Z. Zhang, W. Zhang, J. Wang, H. Chen, M. Li, J. Alloys Compd. **872**, 159707 (2021); https://doi.org/10.1016/j.jallcom.2021.159707
[14] A. V. Egorysheva, V. D. Volodin, T. Milenov, P. Rafailov, V. M. Skorikov, T. D. Dudkina, Russ. J. Inorg. Chem. **55**, 1810 (2010); https://doi.org/10.1134/S0036023610110185
[15] E. V. Karasik, Yu. S. Hordieiev, Voprosy Khimii i Khimicheskoi Tekhnologii **6**, 69 (2020); https://doi.org/10.32434/0321-4095-2020-133-6-69-74
[16] Y. Hordieiev, A. Zaichuk, Thermal and crystallization behavior of aluminum-doped bismuth borate glasses, MRS Advances (2024); https://doi.org/10.1557/s43580-024-00820-5
[17] Yu. S. Hordieiev, A. V. Zaichuk, Chalcogenide Lett. **21**(3), 243 (2024); https://doi.org/10.15251/CL.2024.213.243
[18] Yu. S. Hordieiev, A. V. Zaichuk, Chalcogenide Lett. **19**(12), 891 (2022); https://doi.org/10.15251/CL.2022.1912.891
[19] C. P. E. Varsamis, N. Makris, C. Valvi, E. I. Kamitsos, Phys. Chem. Chem. Phys. **23**, 10006 (2021); https://doi.org/10.1039/D1CP00301A
[20] A. H. Hammad, M. A. Marzouk, H. A. ElBatal, Silicon. **8**, 123 (2016); https://doi.org/10.1007/s12633-015-9283-x
[21] I. Ardelean, S. Cora, J. Mater. Sci.: Mater. Electron. **19**, 584 (2008); https://doi.org/10.1007/s10854-007-9393-3
[22] P. Pascuta, G. Borodi, M. Bosca, L. Pop, S. Rada, E. Culea, J. Phys. Conf. Ser. **182**, 012072 (2009); https://doi.org/10.1088/1742-6596/182/1/012072
[23] Y. S. Hordieiev, A. V. Zaichuk, J. Ovonic. Res. **19**, 471 (2023); https://doi.org/10.15251/jor.2023.194.471

[24] E. R. Shaaban, M. Shapaan, Y. B. Saddeek, J. Phys. Condens. Matter. **20**, 155108 (2008); https://doi.org/10.1088/0953-8984/20/15/155108
[25] L. Vijayalakshmi, K. Naveen Kumar, Jong Dae Baek, Journal of Rare Earths **42**, 46 (2024); https://doi.org/10.1016/j.jre.2022.11.007
[26] B. Karthikeyan, C.S. Suchand Sandeep, J. Cha, H. Takebe, R. Philip, S. Mohan, J. Appl. Phys. **103**, 103509 (2008); https://doi.org/10.1063/1.2931029
[27] P. Kaur, K.J. Singh, S. Thakur, P. Singh, B.S. Bajwa, Spectrochim. Acta A Mol. Biomol. Spectrosc. **206**, 367 (2019); https://doi.org/10.1016/j.saa.2018.08.038
[28] S. Ibrahim, F. I. El-Agawany, Y. S. Rammah, E. M. Ahmed, A. A. Ali, Optik (Stuttg.). **243**, 167414 (2021); https://doi.org/10.1016/j.ijleo.2021.167414
[29] R. Vijaya Kumar, P. Gayathri Pavani, B. Ramesh, M. Shareefuddin, K. Siva Kumar, Opt. Mater. **35**, 2267 (2013); https://doi.org/10.1016/j.optmat.2013.06.013
[30] Y. Cheng, H. Xiao, W. Guo, W. Guo, Thermochim. Acta. **444**, 173 (2006); https://doi.org/10.1016/j.tca.2006.03.016
[31] J. E. Shelby, Introduction to Glass Science and Technology, The Royal Society of Chemistry, London, (2020); https://doi.org/10.1039/9781839169229
[32] A. Dietzel, Glasstech Ber. **22**, 41 (1968).
[33] M. Saad, M. Poulain, Mater. Sci. For. **19–20**, 11 (1987); https://doi.org/10.4028/www.scientific.net/msf.19-20.11
[34] A. Hrubý, Czechoslov. J. Phys. **22**, 1187 (1972); https://doi.org/10.1007/bf01690134
[35] W. Kauzmann, Chem. Rev. **43**, 219 (1948); https://doi.org/10.1021/cr60135a002
[36] V. Dimitrov, T. Komatsu, J. Chemi. Technol. Metall. **45**(3), 219 (2010).
[37] M. K. Halimah, A. S. Asyikin, S. N. Nazrin, M. F. Faznny, J. Non Cryst. Solids. **553**, 120467 (2021); https://doi.org/10.1016/j.jnoncrysol.2020.120467
[38] M. H. M. Zaid, K. A. Matori, S. N. Nazrin, M. N. Azlan, R. Hisam, S. M. Iskandar, N. N. Yusof, F. C. Hila, M. I. Sayyed, Opt. Mater. **122**, 111640 (2021); https://doi.org/10.1016/j.optmat.2021.111640
[39] M. M. Soraya, Fatma. B. M. Ahmed, M. M. Mahasen, Journal of Materials Science: Materials in Electronics **33**, 22077 (2022); https://doi.org/10.1007/s10854-022-08971-7